

STRESS DISTRIBUTION IN A LONG CYLINDER UNDER AXIAL LOADS

K. T. SUNDARA RAJA IYENGAR AND N. G. JAYASHREE

(Department of Civil Engineering, Indian Institute of Science, Bangalore 560 012)

Received on August 16, 1976 and in revised form on November 26, 1976

ABSTRACT

In long circular columns under axial loads, the effect of area of load distribution and Poisson's ratio has been studied. The results of the analysis show that the magnitudes of maximum tensile stresses σ_x or σ_y decrease as the load distribution area ϵ increases and also stresses are maximum when the Poisson's ratio is zero. The results are applied for the anchorage zone of a prestressed concrete beam or column.

Key words: Semi-infinite cylinder, stress analysis, end loads, Poisson's ratio effects.

1. INTRODUCTION

The stress distribution in a long solid circular column under loads which are partially distributed over the end surface of the column is a practical problem often encountered in practice. Solutions to such problems for strips have been given by Sundara Raja Iyengar [1] and he has applied this solution to determine the anchorage zone stresses in prestressed concrete [2]. Hiltcher and Florin [3, 4] have applied photoelasticity to the strip problem. However the problem of the cylinder under end loads is a three-dimensional one.

Treating the column as a long one that is, a semi-infinite cylinder, Sundara Raja Iyengar [5] has given a solution and in this paper references to a number of other solutions are given. Recently Hiltcher and Florin [6] have given solutions to the same problem using dynamic relaxation method and they have given results for maximum tensile bursting stresses occurring near the ends. In the present paper, using the solutions derived in ref. [5], detailed stress distributions are given showing the effect of the area of the distribution of load and Poisson's ratio. Some results as applied to the end block of a prestressed concrete beam are compared with those available.

2. SOLUTION

The cylinder with its co-ordinate axes and loading are shown in Fig. 1. The radius of the cylinder is taken as unity. The loading is on a circular area of radius ϵ (when $\epsilon < 1$). Since the stresses near the loaded end are important, the cylinder can be considered to be long enough such that the effect of the other end is not felt near the loaded end. Hence it is considered as a semi-infinite cylinder.

The basic axi-symmetric problem can be formulated in terms of Love's function ϕ satisfying the bi-harmonic equation

$$\nabla^4 \phi = 0 \quad (1)$$

The stresses are

$$\begin{aligned} \sigma_r &= \frac{\partial}{\partial z} \left[\mu \nabla^2 \phi - \frac{\partial^2 \phi}{\partial r^2} \right] \\ \sigma_\theta &= \frac{\partial}{\partial z} \left[\mu \nabla^2 \phi - \frac{1}{r} \frac{\partial \phi}{\partial r} \right] \\ \sigma_z &= \frac{\partial}{\partial z} \left[(2 - \mu) \nabla^2 \phi - \frac{\partial^2 \phi}{\partial z^2} \right] \\ \tau_{rz} &= \frac{\partial}{\partial r} \left[(1 - \mu) \nabla^2 \phi - \frac{\partial^2 \phi}{\partial z^2} \right] \end{aligned} \quad (2)$$

and the radial and axial displacements are

$$\begin{aligned} u &= -\frac{1}{2G} \frac{\partial^2 \phi}{\partial r \partial z} \\ w &= -\frac{1 - \mu}{G} \nabla^2 \phi - \frac{1}{2G} \frac{\partial^2 \phi}{\partial z^2} \end{aligned} \quad (3)$$

where μ and G are Poisson's ratio and shear modulus respectively.

The boundary conditions considered are:

$$\text{On } r = 1, \quad \sigma_r = \tau_{rz} = 0$$

$$\text{On } z = 0, \quad \sigma_z = f(r), \quad \tau_{rz} = 0 \quad (4)$$

where the given $f(r)$ is self-equilibrating, *i.e.*,

$$\int_0^1 f(r) r dr = 0 \quad (5)$$

as $z \rightarrow \infty$, the stresses and displacements vanish. The solution for this basic problem has been derived in ref. (5). Here only the final expressions are given.

$$\begin{aligned}
 \sigma_r &= \sum_{n=1}^{\infty} [D_n (1 - K_n z) - B_n] e^{-K_n z} J_0(K_n r) + \\
 &\sum_{n=1}^{\infty} [(D_n (2\mu + K_n z - 1) + B_n) e^{-K_n z} \frac{J_1(K_n r)}{K_n r} - \\
 &\int_0^{\infty} C(\alpha) \left[\left\{ 1 + \alpha \frac{I_0(\alpha)}{I_1(\alpha)} \right\} I_0(\alpha r) - \left\{ \alpha r \frac{I_0(\alpha)}{I_1(\alpha)} - 2(1 - \mu) \right\} \right. \\
 &\quad \left. I_1(\alpha r) \right] \cos \alpha z d\alpha \\
 \sigma_\theta &= 2\mu \sum_{n=1}^{\infty} D_n e^{-K_n z} J_0(K_n r) + \sum_{n=1}^{\infty} [D_n (1 - 2\mu - K_n z) - B_n] \\
 &e^{-K_n z} \frac{J_1(K_n r)}{K_n r} + \int_0^{\infty} C(\alpha) [(1 - 2\mu) I_0(\alpha r) \\
 &\quad - \left\{ \alpha \frac{I_0(\alpha)}{I_1(\alpha)} - 2(1 - \mu) \right\} \frac{I_1(\alpha r)}{\alpha r}] \cos \alpha z d\alpha \quad (6) \\
 \sigma_z &= \sum_{n=0}^{\infty} [D_n (1 + K_n z) + B_n] e^{-K_n z} J_0(K_n r) \\
 &\quad + \int_0^{\infty} C(\alpha) \left[\left\{ \frac{I_0(\alpha)}{I_1(\alpha)} - 2 \right\} I_0(\alpha r) - \alpha r I_1(\alpha r) \right] \cos \alpha z d\alpha \\
 \tau_{rz} &= \sum_{n=1}^{\infty} [K_n z D_n + B_n] e^{-K_n z} J_1(K_n r) \\
 &\quad - \int_0^{\infty} C(\alpha) [\alpha r I_0(\alpha r) - \alpha \frac{I_0(\alpha)}{I_1(\alpha)} - I_1(\alpha r)] \sin \alpha z d\alpha \\
 u &= -\frac{1 + \mu}{E} \sum_{n=1}^{\infty} [D_n (2\mu + K_n z - 1) + B_n] e^{-K_n z} \frac{J_1(K_n r)}{K_n} \\
 &\quad - \frac{1 + \mu}{E} \int_0^{\infty} \frac{C(\alpha)}{\alpha} [-\alpha r I_0(\alpha r)
 \end{aligned}$$

$$+ \left\{ \alpha \frac{I_0(\alpha)}{I_1(\alpha)} + 2(1 - \mu) \right\} I_1(\alpha r) \cos \alpha z da$$

and

$$w = \frac{1 - \mu}{E} \sum_{n=1}^{\infty} [D_n (2\mu - 2 - K_n^{-2}) - b_n] \frac{I_0(\epsilon K_n r)}{K_n} \\ + \frac{1 - \mu}{E} \int_0^{\infty} C(\alpha) \left[\left\{ \alpha \frac{I_0(\alpha)}{I_1(\alpha)} + 2(1 - \mu) \right\} I_0(\alpha r) \right. \\ \left. - \alpha r I_1(\alpha r) \right] \sin \alpha z da \quad (7)$$

where the summation in the series is taken over the roots of $J_1(K_n) = 0$ excluding $K_n = 0$, $I_0(\alpha r)$ and $I_1(\alpha r)$ are the modified Bessel functions of the first kind and of the zero and first order respectively.

The constants B_n , D_n and the function $C(\alpha)$ are determined for the boundary conditions (4) [Ref. 5].

3. NUMERICAL RESULTS

Numerical results are obtained for the following problems: A long cylinder is loaded on the end face by a normal load P distributed over a radius ϵ ($\epsilon < 1$) as shown in Fig. 1. By removing the average compressive stress $q = \frac{P}{\pi}$, from the applied loading, radially symmetric self-equilibrating normal stress distribution is obtained on the end face and for this problem, the solution given above is applied. To this solution the stress $\sigma_z = -q$ must be added to obtain the final distribution. In this case,

$$A_n = - \frac{2q J_1(\epsilon K_n)}{\epsilon K_n J_0^2(K_n)} \quad (8)$$

It has been shown in ref. (5) that for 16 terms in the series the convergence is very good. Stresses have been evaluated at different locations for various areas of load distribution (ϵ). To determine the effect of Poisson's ratio on the stress distribution three values of Poisson's ratio have been considered $\mu = 0, 0.2, 0.3$.

4. PRESENTATION OF RESULTS

The numerical results are presented to determine

- (i) the effect of the area of load distribution (ϵ) at the end.
- (ii) the effect of Poisson's ratio (μ).

(i) *Effect of Load Distribution*

Figures 2 and 3 give the radial stress non-dimensionalised with respect to q , along longitudinal sections $r = 0$, $r = 0.2$ and $r = 0.8$ for $\mu = 0.2$ for values of ϵ ranging from 0.1 to 0.9. The distribution of tangential stress σ_θ are shown in Fig. 4 for different values of ϵ and $\mu = 0.2$ along $r = 1.0$. Due to symmetry $\sigma_\theta = \sigma_r$ along the central axis (*i.e.*, $r = 0$). The distribution of axial stress σ_z along $r = 0, 0.2$ and 1 are shown in Figs. 5 and 6. The shear stress distribution at $r = 0.2$ and 0.4 are shown in Fig. 7.

(ii) *Effect of Poisson's Ratio*

Figure 8 shows the distribution of σ_r for the three different Poisson's ratios along $r = 0$ for $\epsilon = 0.2$ and 0.5. Distributions of σ_θ , and σ_z are shown in Figs. 9 to 12. Variation of radial and axial displacements across $z = 0$ are shown in Figs. 13 and 14.

TABLE I

Variation of magnitude of max. tensile stress (radial) at $r = 0$

ϵ	$\mu = 0.3$	$\mu = 0.2$	$\mu = 0.3$	%Differences between $\mu = 0$ and $\mu = 0.3$	%Differences between $\mu = 0$ and $\mu = 0.2$
0.1	3.7219	1.7688	0.9684	73.981	52.475
0.2	1.1360	0.5715	0.4501	50.389	49.690
0.3	0.5807	0.3764	0.3229	44.394	35.130
0.4	0.3810	0.2952	0.2635	30.839	22.460
0.5	0.2850	0.2328	0.2071	27.587	18.600
0.6	0.2179	0.1767	0.1570	27.948	18.900
0.7	0.1571	0.1274	0.1132	27.943	18.900
0.8	0.1021	0.0830	0.0746	18.707	18.700
0.9	0.0503	0.0411	0.0371	26.240	18.290

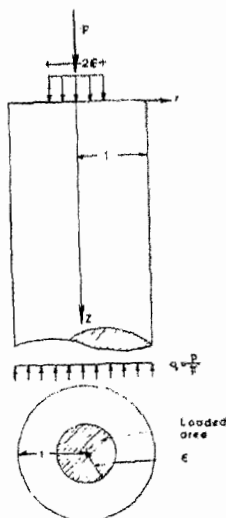
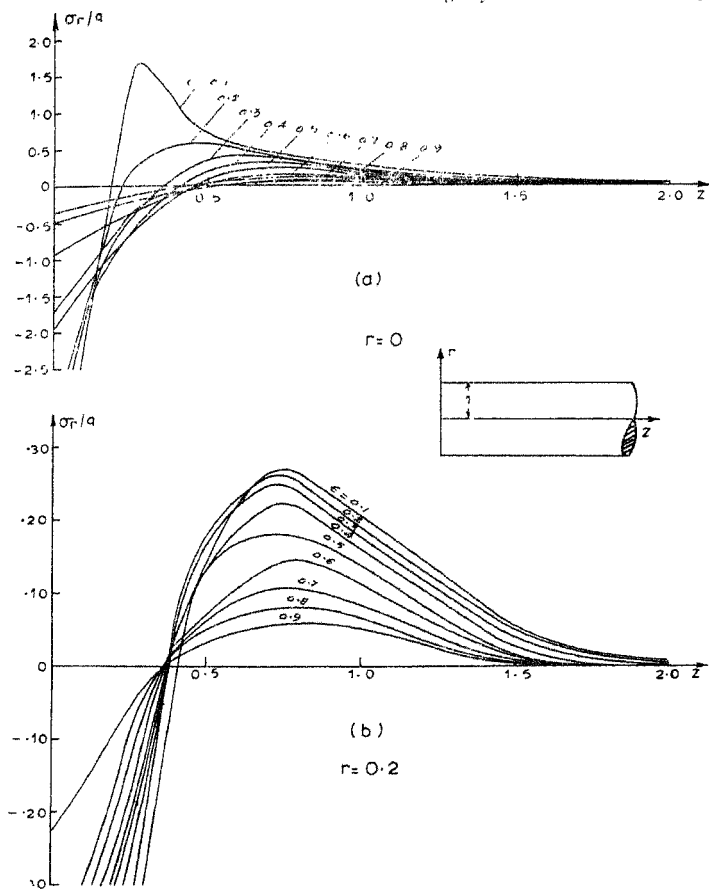


FIG. 1. Co-ordinate axes and the loading system.

TABLE II
Variation of magnitude of max. tensile (tangential stresses) at $r = 0.2$

ϵ	$\mu = 0$	$\mu = 0.2$	$\mu = 0.3$	% Differences between $\mu = 0$ and $\mu = 0.3$	% Differences between $\mu = 0$ and $\mu = 0.2$
0.1	0.9857	0.6596	0.5234	46.900	33.083
0.2	0.6522	0.4937	0.4153	36.323	24.300
0.3	0.4969	0.3537	0.3172	36.164	28.810
0.4	0.3479	0.2886	0.2641	24.087	17.045
0.5	0.2740	0.2318	0.2115	22.810	15.400
0.6	0.2120	0.1787	0.1628	23.207	15.700
0.7	0.1547	0.1303	0.1115	27.925	15.770
0.8	0.1040	0.0856	0.0781	25.000	17.690
0.9	0.0503	0.0426	0.0390	21.465	15.700

FIG. 2. Distribution of radial stress ($\mu = 0.2$).

5. DISCUSSION OF RESULTS

From the results presented in the previous figures, the following conclusions can be drawn:

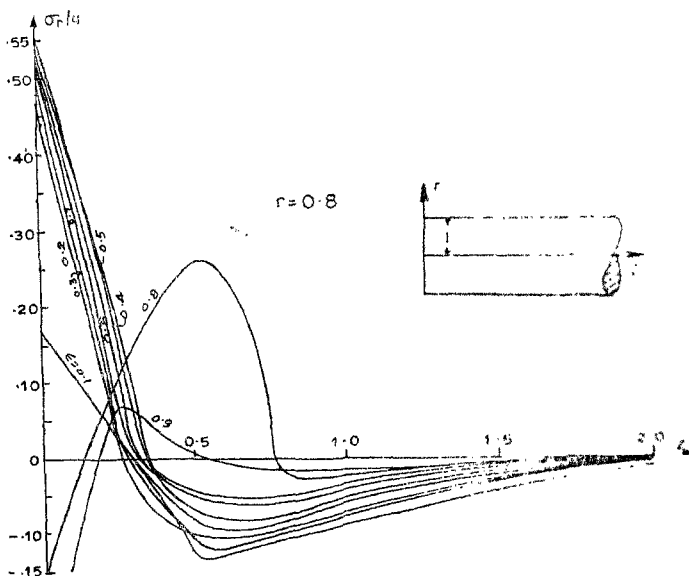


FIG. 3. Distribution of radial stress ($\mu = 0.2$).

(i) Along the central axis, the magnitudes of the maximum tensile stress σ_r or σ_θ decrease as the load distribution area increases.

This is true for all the horizontal sections where the tensile region is away from the end face. As can be seen from Fig. 3 near the curved boundary there are two regions where the tensile stresses can occur depending on the value of ϵ .

(ii) Maximum tensile stress σ_θ also decreases with increasing value of ϵ on all horizontal sections.

(iii) Longitudinal stress σ_z becomes uniform at a distance of about twice the radius of the cylinder and on the curved edge $r = 1$, the stresses are tensile in nature for all values of ϵ (Fig. 6).

(iv) The maximum shear stress value decreases with increase in value of ϵ along $r = 0$ and $r = 0.4$.

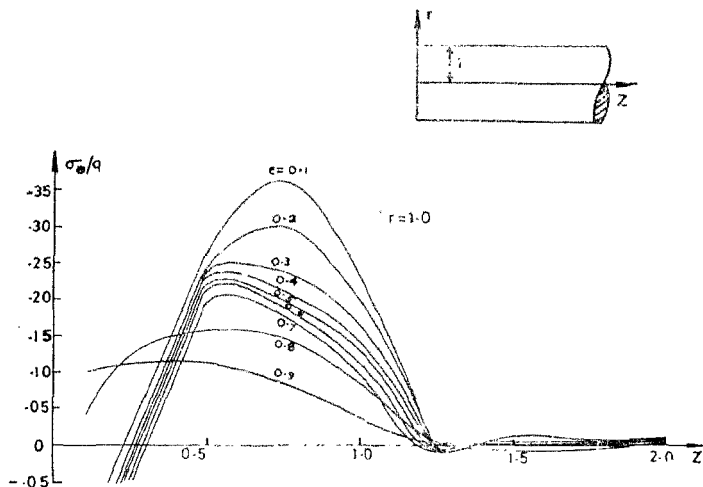


FIG. 4. Distribution of hoop stress σ_{θ} ($\mu = 0.2$).

(v) From a consideration of all the stress components in a long cylinder with concentric loading on the end face, the St. Venant's zone is limited to a length equal to the diameter of the cylinder.

(vi) Since this problem is a three-dimensional one Poisson's ratio will have an effect on the stress distribution. This can be clearly seen in Figs 8 to 14. The maximum tensile transverse stresses σ_r and σ_{θ} decrease as μ increases from 0 to 0.3 except for σ_{θ} near the boundary where the trend is otherwise (Fig. 10). The value of the longitudinal stress σ_z (Fig. 11) decreases as μ increases. On the boundary $r = 1$, the maximum tensile stress σ_z is higher for higher value of μ . Along the loaded end ($z = 0$), the radial displacement is higher for $\mu = 0$ and it decreases as μ increases.

Tables I and II indicate the percentage difference in magnitude of maximum tensile stresses σ_r and σ_{θ} for different load distribution areas (ϵ) for Poisson's ratios $\mu = 0$ and $\mu = 0.2$, and $\mu = 0$ and 0.3 . It can be seen that the magnitudes of the tensile (max.) stresses are greater at $\mu = 0$ than at $\mu = 0.2$. The percentage difference is maximum for $\epsilon = 0.1$ (for both radial and tangential stresses) and decreases as load distribution area increases

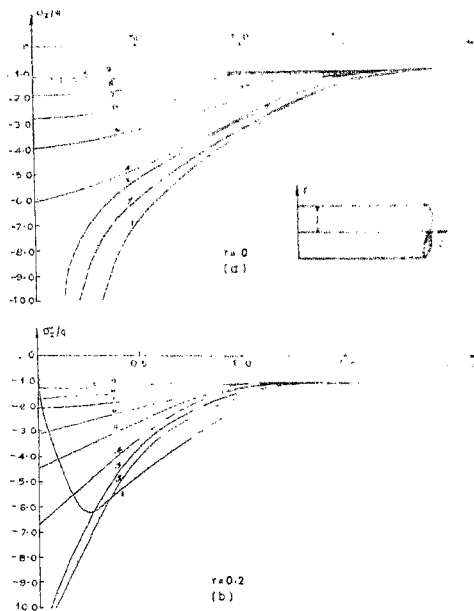
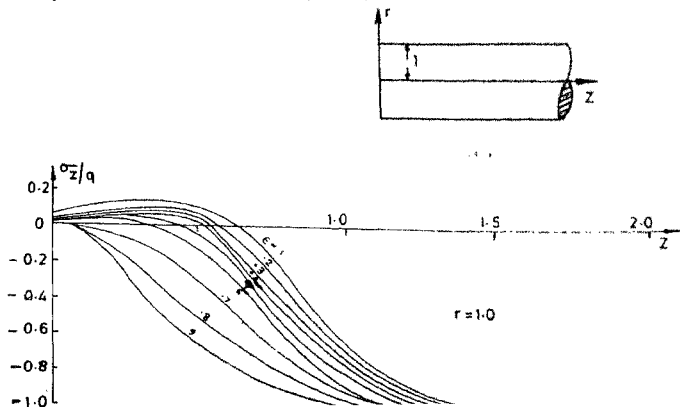


FIG. 5. Distribution of axial stress ($\mu = 0.2$).



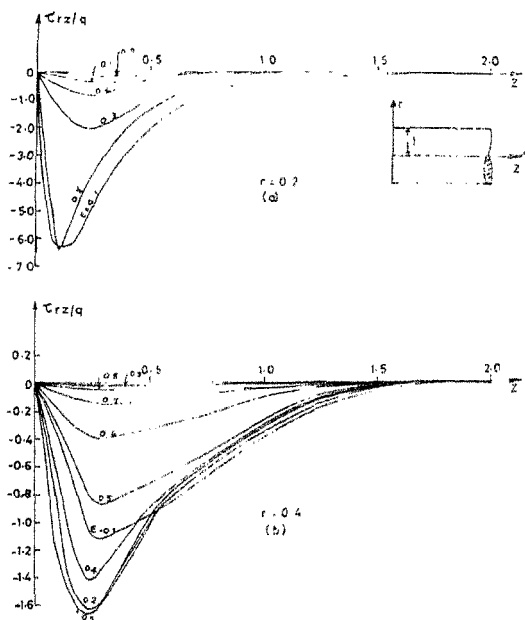


FIG. 7. Distribution of shear stress τ_{rz} ($\mu = 0.2$).

(for radial stress). There is no significant difference in % difference of the stresses for $\epsilon = 0.5$ to 0.9 . For both the stresses, the maximum difference is at $\epsilon = 0.1$ and minimum at $\epsilon = 0.9$. Since the magnitude of the tensile stresses are greater at $\mu = 0$, for all practical purposes μ can be assumed as zero.

6. APPLICATION OF THE SOLUTION

The solution derived in the foregoing problem can be applied to the problem of long circular concrete columns under axial loads applied over a part of the end face and also to determine the stress distribution in the

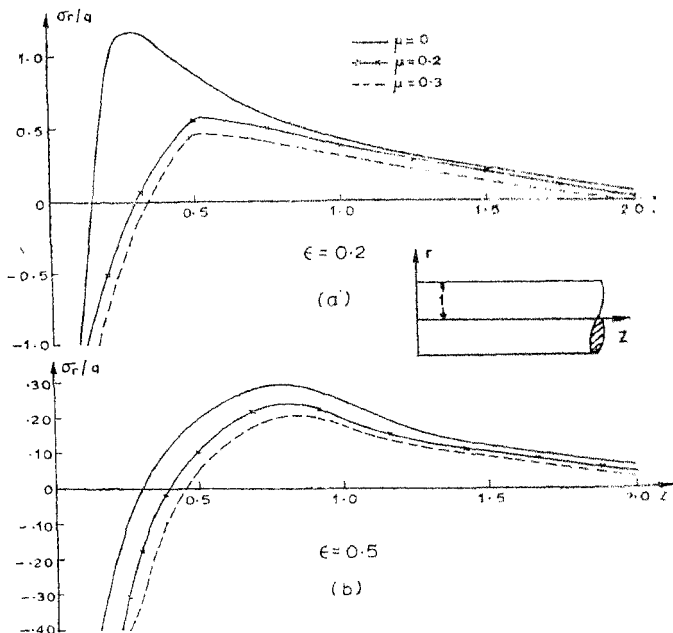


FIG. 8. Variation of radial stress σ_r with Poisson's ratio ($r = 0$).

anchorage zone of the post-tensioned prestressed concrete beam or column. Since concrete is weak in tension, to reinforce it properly the positions of maximum tensile stresses and the tensile zones are to be determined. Figs. 15 and 16 show the magnitudes of maximum tensile (radial and hoop) stresses, positions of maximum tensile stress, and zero stress for $\mu = 0, 0.2$ and 0.3 at $r = 0$ (for radial stress) and $r = 0.2$ (for hoop stress).

The above results may be used in determining the anchorage zone stresses in a prestressed concrete beam.

The three-dimensional problems of stress distribution in the anchorage zone of the post-tensioned pre-stressed concrete beam have been solved in

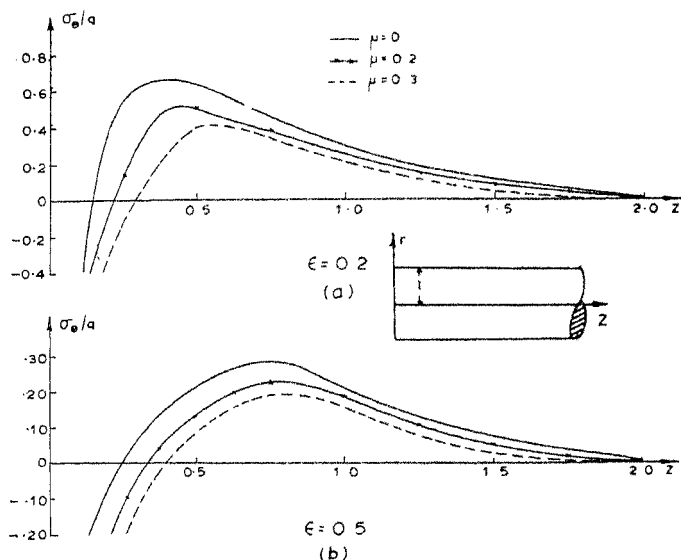


Fig. 9. Variation of hoop stress σ_{θ} with Poisson's ratio ($r = 0.2$).

ref. [7, 8]. The elasticity solution presented in this paper for the semi-infinite cylinder satisfies all the boundary conditions and hence the results can be made use of to obtain the stresses in the anchorage zone and for comparison with other theories [2, 7, 8].

7. DISCUSSION OF THE RESULTS

Figures 15 and 16 indicate that the position of the maximum (radial and hoop) tensile stress and the position of zero stress (radial) shift towards the loading end as load distribution area ϵ is decreased. The magnitude of the maximum tensile (radial and hoop) stress increases as the Poisson's ratio increases. The position of the maximum tensile stress (radial and hoop) and the position of zero stress (radial) shift towards the loading end as Poisson's ratio decreases. There is not much variation in the position of zero stress for hoop (tensile) stress for change of ϵ and μ .

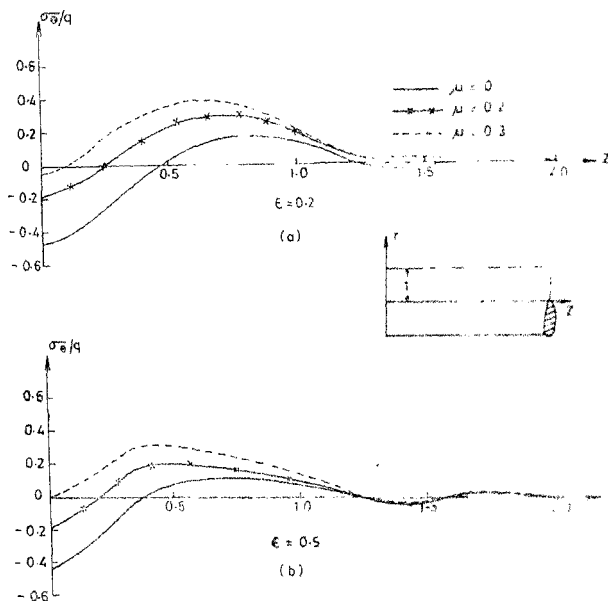


FIG. 10. Variation of hoop stress σ_{θ} with Poisson's ratio ($\nu = 1.0$).

Figure 17 shows the contours of the transverse stress obtained for the semi-infinite cylinder for the value of $\epsilon = 0.2$. Such contours for other two and three-dimensional problems have been given in ref. [7]. Figure 18 shows the magnitude of the maximum tensile stresses for different loading areas for the semi-infinite cylinder and the two other problems shown in Fig. 19. It can be observed that in this solution both the radial and tangential stresses can be thought of as transverse stresses. Hence it can be seen from Fig. 17 that spalling zone exists if radial stress is considered as the one corresponding to σ_y of the three-dimensional rectangular prism. Similar results exist even

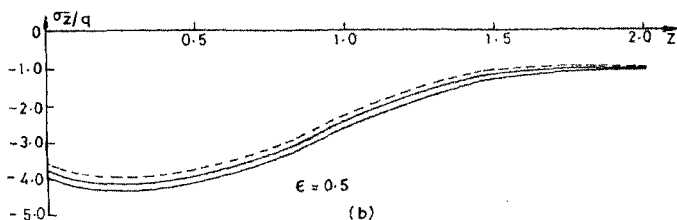
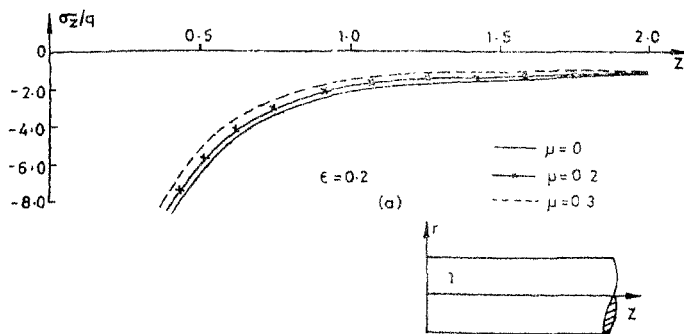


FIG. 11. Variation of axial stress σ_z with Poisson's ratio ($r = 0$).

in the problem of a hollow cylinder [7]. From the foregoing discussion the following conclusions can be drawn:

(1) The magnitude of the maximum transverse tensile stress is less than the three-dimensional prism solution, when the ratio of the loading area to the cross-sectional area (ϵ^2) is less than 0.4 and beyond 0.4, both the results agree with each other (Fig. 18 a).

(2) For $\epsilon^2 > 0.2$, the two-dimensional results give higher value for the maximum tensile stress than that of the prism or present solution (Fig. 18 a).

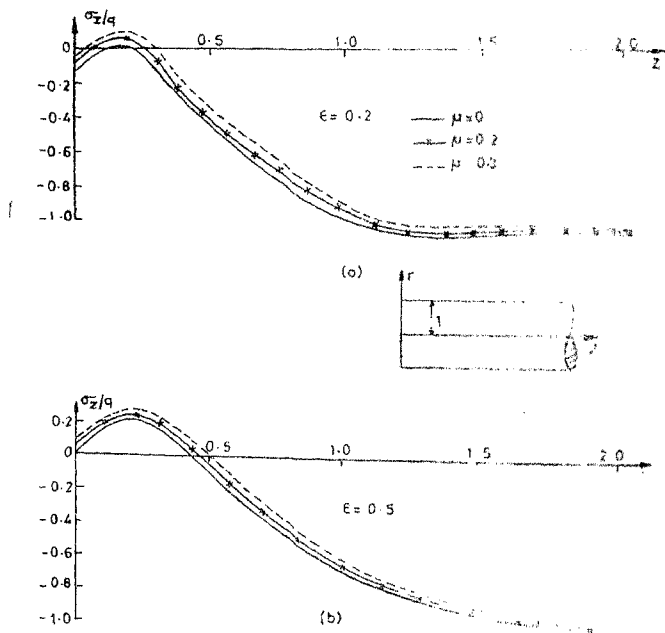


FIG. 12. Variation of axial stress σ_z with Poisson's ratio ($\nu = 1.0$).

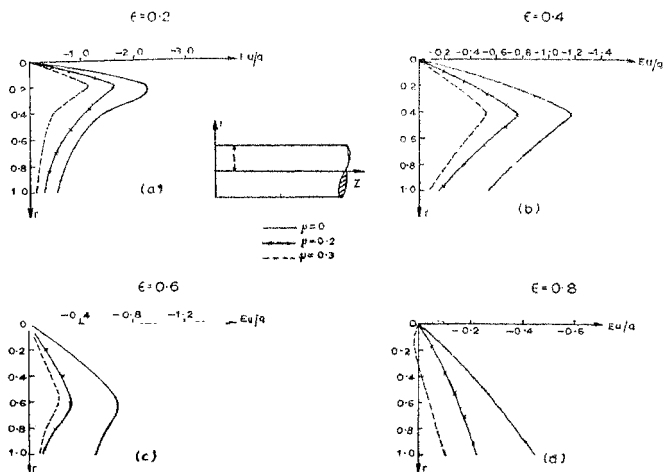


FIG. 13. Variation of radial displacement u with Poisson's ratio across the cross section at $Z=0$.

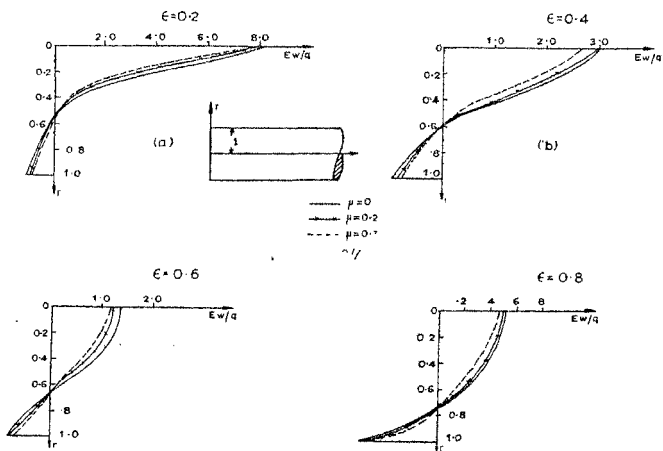


FIG. 14. Variation of axial displacement w with Poisson's ratio along the radius at $Z=0$

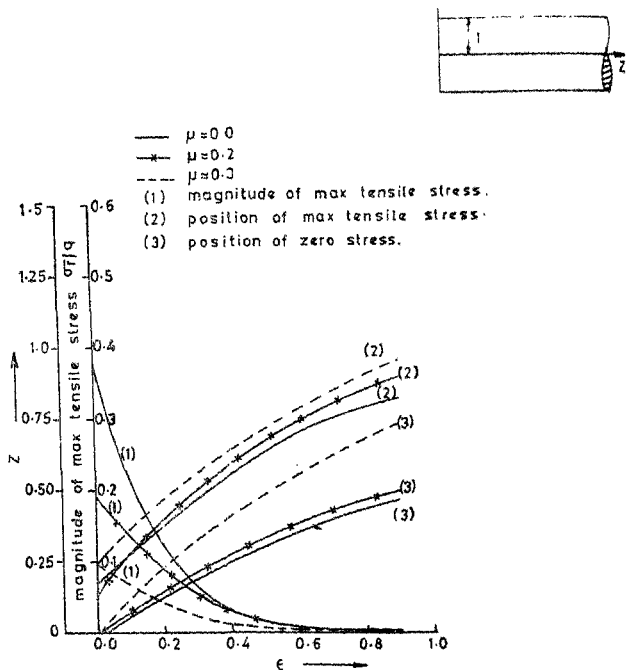


FIG. 15. Variation of radial stress with Poisson's ratio ($r = 0$).

If ϵ is assumed to correspond to β (Fig. 19), the magnitude of the maximum tensile stress in the axisymmetric problem is greater than that obtained by the three-dimensional solution (Fig. 18 *b*). For $\epsilon > 0.3$, the results of the present solution agree with those of the two-dimensional solution.

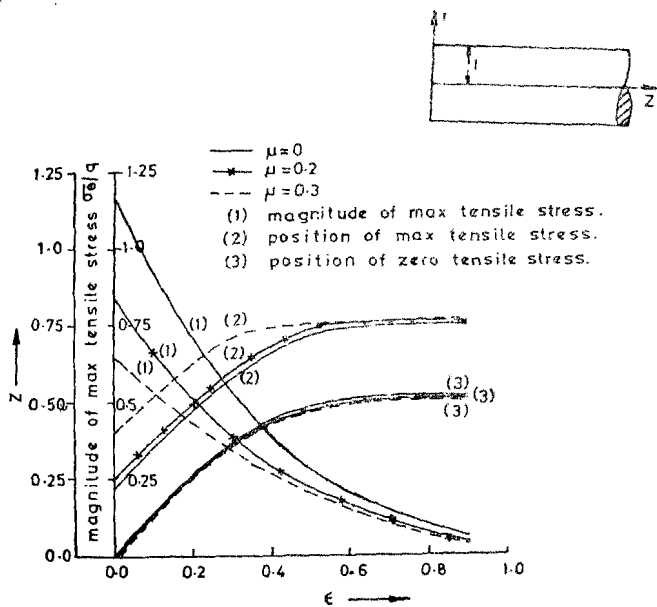


FIG. 16. Variation of hoop stress with Poisson's ratio ($\nu = 0.2$).

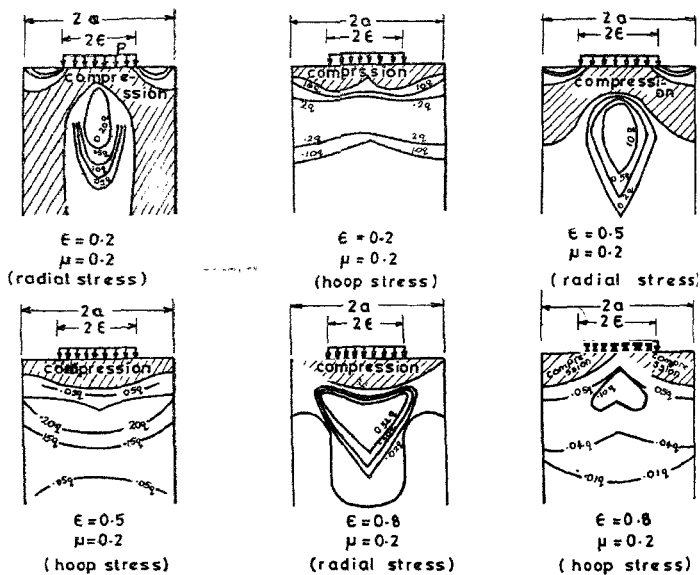


FIG. 17. Transverse stress contours in the anchorage zone (semi-infinite cylinder).

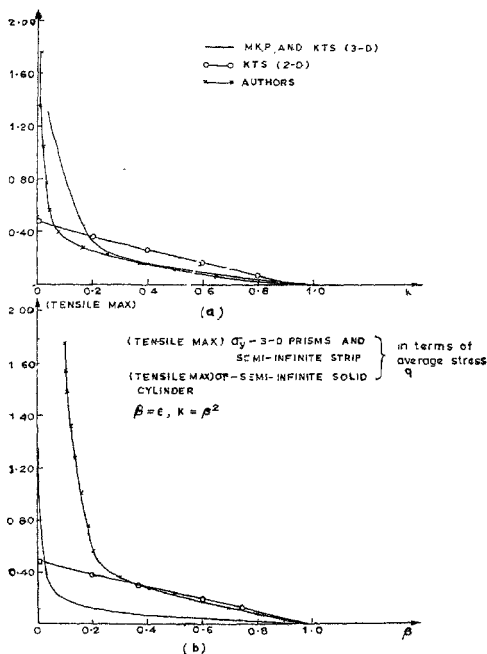


FIG. 18. Magnitude of max tensile stress (σ_r) along the loading axis for different k (loading area).

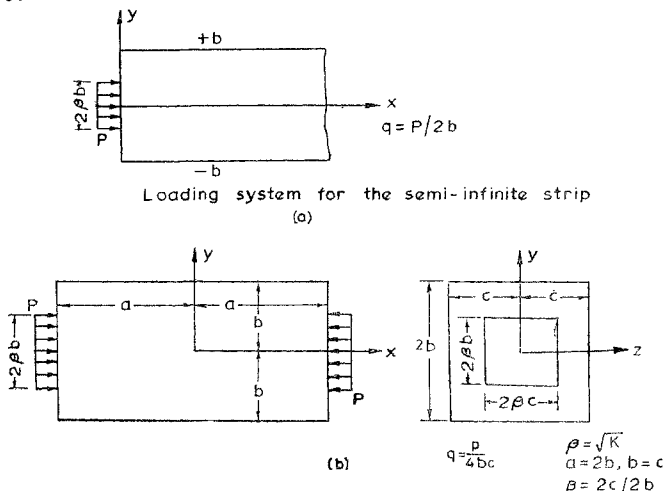


FIG. 19. Loading system for the rectangular prism.

REFERENCES

- [1] Sundara Raja Iyengar, K. T. Über den spannungszustand in einem elastischen Halbstreifen, *Österreichisches Ingenieur Archiv*, 1962, **16** (3) 185-199.
- [2] Sundara Raja Iyengar, K. T. Two-dimensional theories of anchorage zone stresses in post-tensioned prestressed beams, *Journal of American Concrete Institute*, 1962, **59**, 1443-1466.
- [3] Hiltcher, R. and Florin, G. Die spaltzugkraft in einseitig eingespannten, am gegenüber liegenden Rande belasteten rechteckigen Scheiben, *Die Bautechnik*, 1962, **39**, 325-329.
- [4] Hiltcher, R. and Florin, G. Spalt- und Abreisszugspannungen in rechteckigen Scheiben, die durch eine Last in verschiedenem Abstand von einer Scheibenecke belastet sind, *Die Bautechnik*, 1963, **40**, 401-408.
- [5] Sundara Raja Iyengar, K. T. On the end problem of cylinders, *Proceedings of the 1st Australasian Conference on Mechanics of Structures and Materials*. Sydney, 1961, pp. 113-131.
- [6] Hiltcher, R. and Florin, G. Spaltzugspannungen in Kreiszyllindrischen Säulen, die durch eine kreisförmige Flächenlast Zentrisch-axial belastet sind, *Die Bautechnik*, 1972, **49**, 90-94.
- [7] Sundara Raja Iyengar, K. T. and Yogananda, C. V. A three-dimensional stress distribution problem in the anchorage zone of a post-tensioned prestressed concrete beam, *Magazine of Concrete Research*, 1966, **18** (55), 75-84.
- [8] Sundara Raja Iyengar, K. T. and Prabhakara, M. K. A three-dimensional elasticity solution for a rectangular prism under end loads, *ZAMM*, 1969, **49**, 321-333.